



HAL
open science

Numerical Modeling of the Micromechanics Damage of an Offshore Electrical High-Voltage Phase

Fouad Ech-Cheikh, Monssef Drissi-Habti

► **To cite this version:**

Fouad Ech-Cheikh, Monssef Drissi-Habti. Numerical Modeling of the Micromechanics Damage of an Offshore Electrical High-Voltage Phase. *Energies*, 2023, 16 (14), pp.5422. 10.3390/en16145422 . hal-04456440

HAL Id: hal-04456440

<https://hal.science/hal-04456440>

Submitted on 14 Feb 2024

HAL is a multi-disciplinary open access archive for the deposit and dissemination of scientific research documents, whether they are published or not. The documents may come from teaching and research institutions in France or abroad, or from public or private research centers.

L'archive ouverte pluridisciplinaire **HAL**, est destinée au dépôt et à la diffusion de documents scientifiques de niveau recherche, publiés ou non, émanant des établissements d'enseignement et de recherche français ou étrangers, des laboratoires publics ou privés.



energies



Article

Numerical Modeling of the Micromechanics Damage of an Offshore Electrical High-Voltage Phase

Fouad Ech-Cheikh and Monssef Drissi-Habti



<https://doi.org/10.3390/en16145422>

Article

Numerical Modeling of the Micromechanics Damage of an Offshore Electrical High-Voltage Phase

Fouad Ech-Cheikh and Monsef Drissi-Habti * 

Cosys Department, Université Gustave Eiffel, F-77447 Marne-la-Vallée, France

* Correspondence: monsef.drissi-habti@univ-eiffel.fr

Abstract: Due to the strong growth of offshore renewable energies, research and engineering in this field is constantly expanding. One of the centerpieces of these technologies is the high-voltage electrical cable, generally made of copper, to transport the energy produced from the offshore farm to the onshore station. The critical nature of these cables lies in the proven resistance that they must demonstrate during stays underwater for several years, even decades, in difficult environmental conditions, which begin at the handling, shipping and underground burial stage. The marine environment can lead to deformation of the copper wires well beyond the limit of proportionality and, consequently, to breakage. Copper, although being an exceptional electrical conductor, has very poor mechanical properties. The plasticity generated by the excessive deformation of copper wires affects all of the physical properties of copper. When plasticity develops, electrical transport is affected and the heat within copper increases, but care should be given to not exceed 90 °C, as this would result in the shutdown of the cable with dramatic economic consequences. The work carried out in this article, which is part of the National Project EMODI as well as the European Project FLOW-CAM, aims at studying the mechanical behavior of the phase in order to correlate the deformation levels reached to the phase geometry as well as operating mechanisms of damage which reflect the proliferation of microstructural defects within the conductor. To do this, we propose a numerical model using Abaqus. Correct description of the effects of several parameters (geometry of the phase) and plasticity development on the performance of the phase were simulated and discussed.



Citation: Ech-Cheikh, F.; Drissi-Habti, M. Numerical Modeling of the Micromechanics Damage of an Offshore Electrical High-Voltage Phase. *Energies* **2023**, *16*, 5422. <https://doi.org/10.3390/en16145422>

Academic Editor: Francesco Castellani

Received: 9 May 2023

Revised: 7 June 2023

Accepted: 7 July 2023

Published: 17 July 2023



Copyright: © 2023 by the authors. Licensee MDPI, Basel, Switzerland. This article is an open access article distributed under the terms and conditions of the Creative Commons Attribution (CC BY) license (<https://creativecommons.org/licenses/by/4.0/>).

Keywords: numerical simulation; electrical hi-voltage cable; offshore; mechanical behavior; micro-mechanics

1. Introduction

The development of renewable energy sources such as offshore wind energy becomes a necessity nowadays. This renewable energy source is expected to reach 450 GW by 2050, if Europe wants to meet carbon neutrality. This energy source is an alternative resource whose growth is most spectacular, particularly in Europe and Asia. Its generation is organized in offshore wind farms. Targeting 450 GW for Europe requires an appropriate strategy that is based on set-up of reliable infrastructure (wind turbines, electric high-voltage cables, etc.) and this is a hot topic [1–5]. Moreover, the maintenance of these structures is also a major concern [1–5]. High-voltage electric cables are critical structures that must ensure reliable electric transport ashore over at least 20 years. The steps of production, shipping, handling and placement on the seabed of high voltage electric cables can cause damage and therefore partially affect their qualities. These steps with their hazards come as a prelude to very difficult work constraints in a very humid, very saline environment, subject to sometimes very strong currents, to shocks, aquatic animals, to a very steep and therefore “unfriendly” marine topography and therefore to fear of premature termination. All this can lead to large budgetary expenditures, as well as geopolitical problems, with serious consequences. Just as important as O&M expenses, cable failures account for 80% of the total financial loss envelope. insurance claims. Over the past few years, around a hundred

breakdowns and/or failures have been recorded for a total loss (claimed against insurance) in excess of 350 million euros. The repair costs of an offshore cable range between 0.7 to 1.5 million euros [6]. The generation of electrical energy is central to any ecological and economic strategy. Policies geared toward sustainability are moving heavily to value safe, clean and sustainable energy sources. However, it should be borne in mind that the investment and maintenance costs of offshore wind farms are very high. Very substantial losses are to be feared in the event of a production breakdown, due in particular to the very difficult access for interventions in the marine environment, in the event of heavy maintenance, using specific equipment (boats, helicopters, etc.), highly skilled workers and requiring supportive weather conditions. The concomitance of the aforementioned factors leads to long, even very long maintenance times, and this can be a real limitation on profitability. The above proves beyond any doubt that it is essential to monitor live (strain, temperature, etc.) and very precisely what is going on inside HV cables, through appropriate embedded sensors (strain and temperature of copper), and by using fiber-optic sensors (FOS) [2–4]. The excessive plasticity of copper is also responsible for the loss of performance of cables, which occurs even at very low deformations and under very low loads which has a direct influence on the other physical properties. What is important to note in a preliminary way is that the micro-mechanisms of damage operating in a cable with steel wires are fundamentally different in the case of cables with copper wires, even if the denominations are identical. Indeed, copper is a mechanically very soft material, although an excellent electrical conductor. As a result, inter-wire friction results much more in generalized plastic deformation than in wire breakage (in contrast to the case of steel wires where plasticity will be less extensive and breakages are more likely). The reason why extended plasticity is a problem is simply that it will induce many more breaks in electrical and thermal conduction; the dislocations multiplied by the generalized plasticity are the main causes.

In this work, the mechanical damage mechanisms of the cables were identified and simulated, numerically. The work was carried out on a high voltage phase, in order to reduce the complexity of the calculations. The work carried out aims to study the effects of various damage mechanisms of copper conductor wires on the mechanical behavior. The various damage mechanisms that are simulated are the effects of the coefficient of friction, the winding pitch of the copper wires, work-hardening, local plasticity and failure of a single thread and/or several wires.

2. Numerical Modeling—3D FE Modeling

Before presenting our model, let us first take a look at what is available in the literature. It is worth noting that the models that exist for cables are the ones relating to steel wires, which are extremely different from copper wires when it comes to their mechanical behavior. The first FE models of the cables were built from elements already existing in the NASTRAN code [7]. In 1973 [8], the wires of the cable as well as the connections between wires are modeled by EFs of the “bar” type. In [9], the wires of the cable are modeled by solid elements with 6 nodes but the connections between wires are likened to springs. In 1997 [1], produced a FE model of helical wire (beam model) for the study of the mechanical behavior of a single-strand 1 + 6 cable. In this model, the variation of the diameter of the wires and the local deformations due to the inter-wire contacts (radial contact) are neglected, but the shear force in the section of the wires is considered. Internal friction is also neglected, but all possible inter-wire movements (sliding, rolling and pivoting) are modeled. It is shown there that the inter-filar pivoting is the only inter-wire movement to have a notable influence on the overall response of a cable under axial loading. With the advent of more powerful computers, FE models make it possible to analyze the local and global behavior of the cable in a more realistic and thorough way. In 1996, [10] used the ANSYS code and 3D solid elements with 8 nodes to model a short length of a strand (between 0.1 and 0.35 pitch) of type 1 + 6 in static axial loading. This study is carried out to determine the influence of different parameters on the axial stiffness and the stress distribution between

the outer wires and the core. These parameters are the winding angle of the wires, the boundary conditions in rotation, the length of the model, the radius of the core, the radius of the external wires and the conditions of inter-wire contact (non-slip and sliding total). Reference [11] also used ANSYS code and 8-node solid elements to model 1/12 of a strand (exploiting strand symmetry) of 7 wires subjected to axial loading. They modeled a short length of a strand (approximately 1/1000 of a pitch).

A finite element model which allows us to model the mechanical behavior of our phase with a sufficiently large length and to numerically simulate the various damage mechanisms of the phase was set up using Abaqus [12]. Thanks to this finite element model, non-linear effects such as contact, friction and plasticity, which are very difficult to integrate into an analytical model, are studied. In the following, the steps required to create our FE model on Abaqus are explained. The geometry used in our model is the one shown in Figure 1. This is a layer of 6 threads and of circular section with radius R_w , wound around the core which is also of circular section with radius R_c .

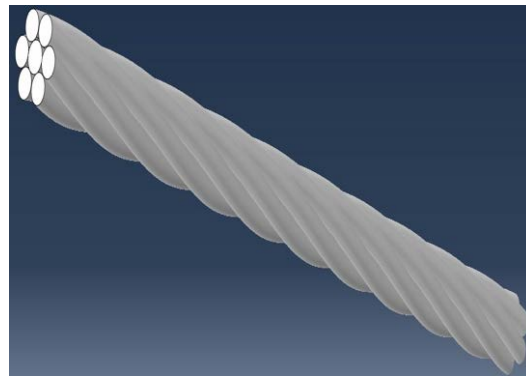


Figure 1. Digitalized phase geometry.

There are two methods used to design this geometry. The first method is to design the core and the 6 helical wires using Abaqus and assemble the two parts to obtain the phase. The second method is to create a program in Python to design the helical wires using parametric equations. The characteristics of the phase geometry are: core radius: $R_c = 1.97$ mm; spiral wire radius: $R_w = 1.865$ mm, pitch: 115 mm. The pitch will be varied to assess the effect on phase behavior. All phase wires are made of copper. The creation of this material on Abaqus is achieved by defining its mechanical behavior (stress–strain). This behavior is defined by two parts, a linear part which represents the elasticity of copper and a non-linear part which represents its plasticity. The elasticity part is characterized by Young’s modulus, E . The behavior is defined by the following Equation [12], where σ is the stress, σ_y the elastic limit of the material, and ε_p is the plastic deformation:

$$\sigma = E\varepsilon \quad (1)$$

In Abaqus [12], a perfectly plastic material (without work-hardening) can be defined and work-hardening can be specified. Isotropic hardening, including Johnson–Cook hardening, is available in Abaqus/Standard and Abaqus/Explicit. Additionally, Abaqus provides kinematic work-hardening for materials under cyclic loading. Perfect plasticity means that the stress does not change with the plastic deformation, i.e., when the stress is lower than the elastic limit, the material has an elastic behavior. When this limit is reached, perfect plasticity can be represented by [12]

$$\sigma = \sigma_y \quad \forall \varepsilon_p > 0 \quad (2)$$

The curve of Figure 2a represents the stress strain curve for a material with perfect plasticity. Isotropic work-hardening means that a homothetic dilatation of the field of elasticity compared to the initial field is supposed to be known. Wherein, the stress is a

function of a tangent modulus E_T for a linear hardening law. The relationship between stresses and strains according to the law of linear hardening can be represented by the graph in Figure 2b. This law can be modeled by the following Equation [12]:

$$\sigma = \sigma_y + E_T \varepsilon_p \quad \forall \varepsilon_p \geq 0 \quad (3)$$

where E_T is the slope of the stress-strain curve, called the tangent modulus. The values of this modulus are expressed in the same units as the Young's modulus. Figure 2c shows another non-linear hardening law which gives the relationship between stresses and strains by the following Equation [12]:

$$\sigma = \sigma_y + K(\varepsilon_p)^n \quad \forall \varepsilon_p \geq 0 \quad (4)$$

where K is the hardness coefficient. The value of this coefficient is greater than 0 but less than Young's modulus; n is the exponent. The exponent is a dimensionless quantity. The exponent value is greater than 0 but less than or equal to 1.

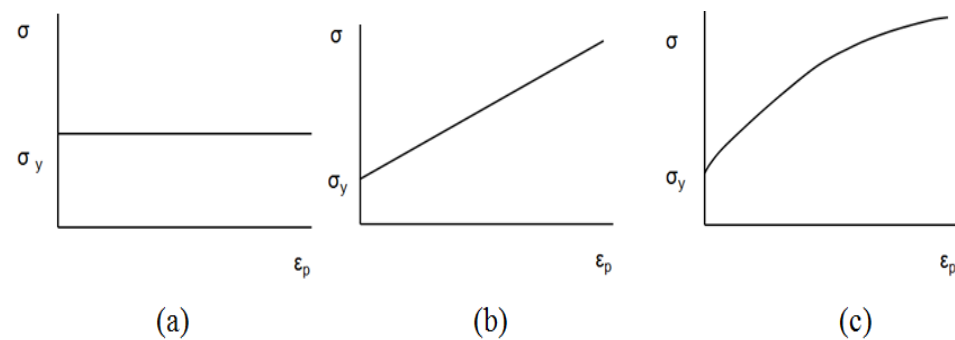


Figure 2. Hardening laws: (a) Perfect plasticity; (b) Linear hardening; (c) Non-linear hardening [12].

The Johnson-Cook model [12] expresses the equivalent stress as a function of 3 material constants, namely plastic deformation, the strain rate and the characteristic temperatures (ambient, transition and melting of the material):

$$\sigma = [A + B\varepsilon^n] \times [1 + C \ln \frac{\dot{\varepsilon}}{\dot{\varepsilon}_0}] \times [1 - \left(\frac{T - T_t}{T_{fusion} - T_t} \right)^m] \quad (5)$$

It is made up, in this order, of an expression of work-hardening, other dynamics and finally thermal softening. The first expression concerning work-hardening translates the flow stress at a constant strain rate. A represents the elastic limit, and B the modulus of work-hardening (linear parameter of work-hardening). The second expression designates the dynamic hardening of the material. This expression is consequent on the speed of plastic deformation and the coefficient C representing the coefficient of dependence on the strain hardening rate. The last term of this law corresponds to the phenomenon of thermal softening taking place from the moment when the temperature of the material is higher than the transition temperature, the coefficient m therefore representing the thermal softening exponent.

The modeled part of the phase (the conductor) is made of homogeneous copper and assumed to be isotropic (although the spinning of the copper puts this assumption into perspective). An elastoplastic model with isotropic work-hardening is defined to model the conductor. The elastic part is defined by Young's modulus, E , and Poisson's ratio, ν , which are 115 GPa and 0.33, respectively. From the stress of 135 MPa which represents the elastic limit of copper, the plastic behavior of copper begins. This behavior is defined by a non-linear isotropic hardening defined by Equation (5). The values of the hardness coefficient K and the work-hardening exponent n for copper are 480 MPa and 0.35, respectively. The

hardening curve obtained from the non-linear hardening model used is entered into Abaqus in the form of a table (plastic stress/strain, Table 1).

Table 1. Stress values are a function of copper plasticity tabulated by us using a power law.

True Stress	Plastic Strain
135	0
144.5	0.00934
160	0.018862
179.5	0.036475
200.4	0.057165
213.5	0.07583
230.5	0.093935
243.4	0.111747
257	0.129062
266.4	0.146372
279.3	0.163696
285	0.180613
306.5	0.212961
316.8	0.245001
328.7	0.276104
340.8	0.291917

2.1. Loading and Boundary Conditions

Three different types of tests were simulated, which are a tensile test, tensile-torsion test and fatigue tests. For all loading cases, one end ($Z = 0$) is clamped, the loading (forces and moments) and the complementary kinematic boundary conditions being imposed at the other end ($Z = L$), depending on the type of test. We applied an axial force for the tensile testing, an axial force and an axial moment for tensile-torsion testing and a cyclic loading for fatigue testing. Two parts were added to the model that consider the jaws of our bench and we applied pressure to the side surface to model the effect of the insulation on the conductor. To apply the loads and boundary conditions at the ends of the conductor, two reference points 1 and 2, shown on Figure 3, were added, located on the axis of the conductor and at a certain distance from the ends. This was introduced in order to couple all nodes of each cross-section to a single node, which facilitates the application of loading and boundary conditions. The coupling defined between the reference point and the cross section kinematically connects the reference point to the cross-section nodes. All the nodes of the section must be rigidly connected to the reference node, i.e., all the nodes of the section (called slave nodes) remain strictly fixed with respect to each other and follow the movement of the reference point. Reference point 1 (RP 1) was fixed and an axial force along the Z axis on reference point 2 (RP 2) was applied, $F_z = 35$ kN for a tensile test. For the tensile-torsion test, a force $F_z = 35$ kN and a rotation along the Z axis ($\theta_z = 0.35$ rad) were applied. For the last test, a cyclic loading was applied. Due to time constraints, we applied cyclic loading with 10 cycles. The cyclic loading shown in Figure 4 is applied to reference point 2 in the z direction.



Figure 3. Reference points of loading.

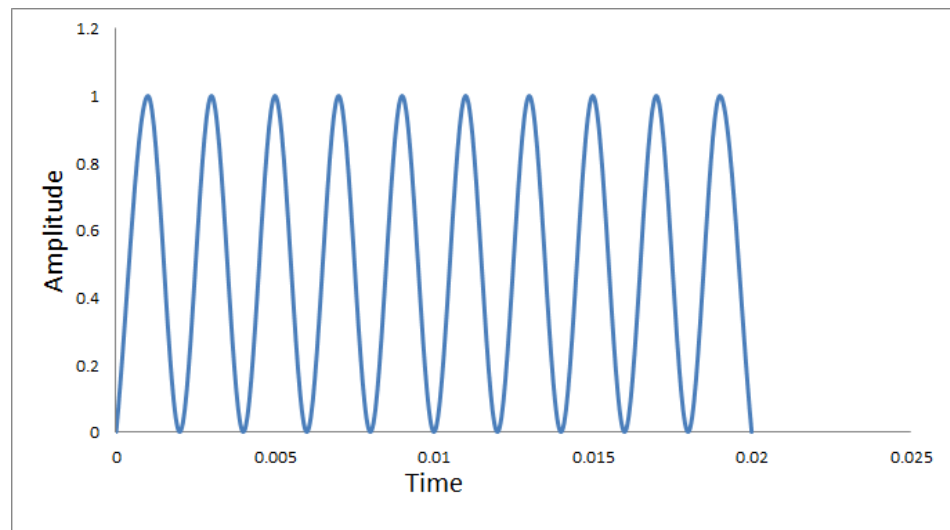


Figure 4. Cyclic loading.

Two loadings are performed, a maximum stress equal to 80% of the elastic limit of the conductor and a maximum stress equal to 100% of the elastic limit of the conductor.

2.2. Meshing

Two types of mesh elements were used for the structural discretization. Linear elements with reduced integration of the C3D8R type, composed of 8 nodes and an integration point, of parallelepipedal shapes, having as degrees of freedom the three displacements in the three directions of space (x, y, z) (Figure 5).

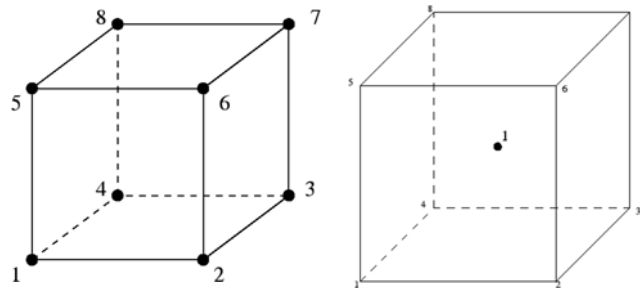


Figure 5. C3D8R Elements with an integration point [12].

Quadratic elements of the C3D20 type were used, composed of 20 nodes and 7 integration points, a center point of the cube and the points at the center of each face. Each node has three displacements in the three directions of space (x, y, z) (Figure 6).

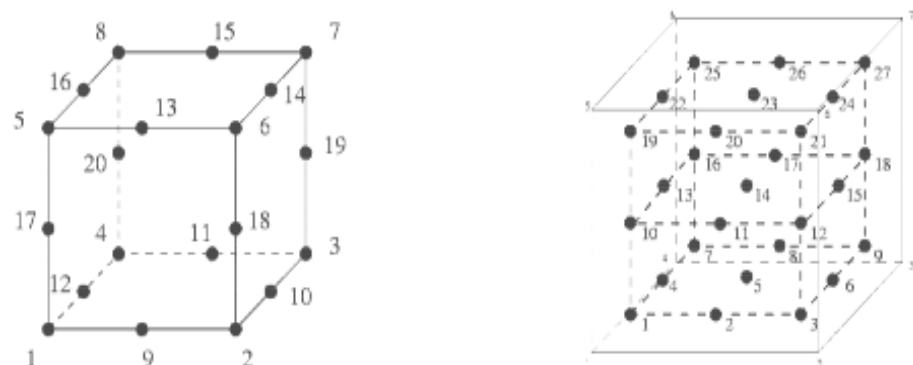


Figure 6. C3D20R elements with corresponding integration points [12].

The elements of contact areas were refined. In total, the problem to be solved is composed of 25252 nodes and 23026 elements (Figure 7).

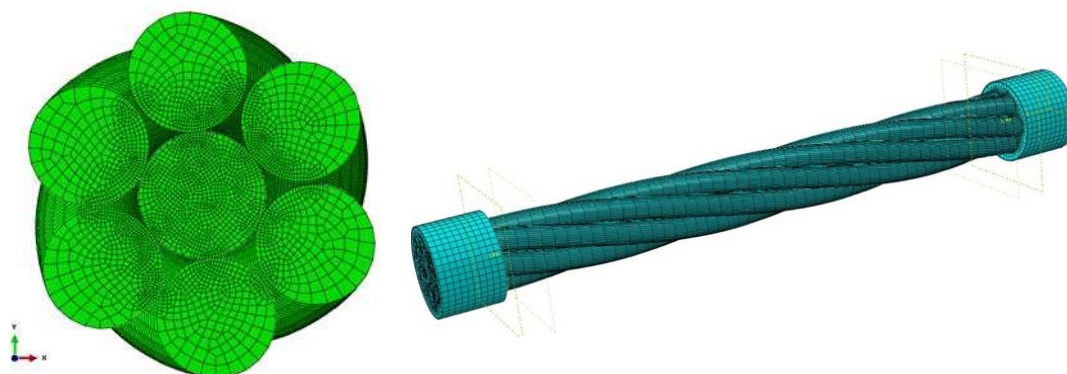


Figure 7. Meshed phase.

2.3. Contact Pressure

The contact between the components of a cable is an important part of modeling. The problem of contact in a cable is complex from a mechanical point of view. In general, two types of contact exist: line contact, which is the contact between the core and the helical wires (Figure 8a), and tangential contact, which is the developed contact between two helical wires (Figure 8b). In most models, the effects of friction and contact strains are neglected.

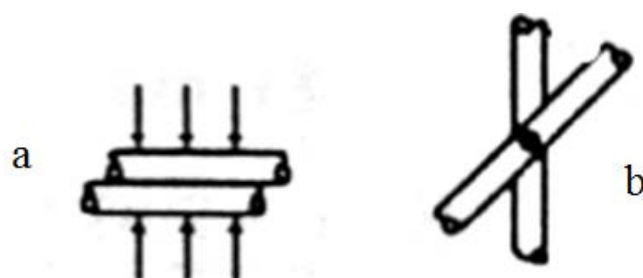


Figure 8. Contact mode in the conductor: (a) lineic, (b) tangential [12].

During axial loading of the conductor, a distributed force X in the normal direction is created. It acts radially inward from the center of each helical wire and creates contact forces. The contact between the central wire (core) and the helical wire can be estimated locally as a contact between two cylindrical bodies (line contact). Since the contact width is very small compared to the radius of the wire, the Hertz theory of contact is applicable [13]. The half-width of the contact a is given according to the properties of the material, the radius of the wire and the linear force of contact as follows (S along the line of contact of each helical wire with the corresponding core) [13].

$$a = 2\sqrt{\frac{2(1-\nu^2)R_w R_c X}{\pi E(R_w + R_c)}} \quad (6)$$

The distribution of contact pressure over the contact width is semi-elliptical, it is expressed by the following Equation [13]:

$$p(\eta) = \frac{2X}{\pi a} \sqrt{1 - \frac{\eta^2}{a^2}} \quad \forall -a \leq \eta \leq a \quad (7)$$

The maximum pressure is for $a = \eta$. This pressure is equal to:

$$P_0 = \frac{2X}{\pi a} = \sqrt{\frac{E(R_c + R_w)X}{2\pi(1 - \nu^2)R_w R_c}} \quad (8)$$

When the slippage of the wires is considered when extending the conductor, the frictional force is added to the normal force. This frictional force can be established by Coulomb's simple law of friction (where T is the frictional force in N; N is the normal force in N and μ is the coefficient of friction) [13]:

$$T = \mu N \quad (9)$$

2.4. Interaction Properties

The interaction module is the most important module in the definition of the contact. This is where the behavior of the surfaces in the model is defined. It defines the mechanical laws that the software must follow to simulate real behavior. From the mechanical point of view, two types of constitutive laws are distinguished: tangential behavior and normal behavior.

There are several contact surfaces in our model. The contact between the phase wires has been defined via the "general contact" in ABAQUS [12], which uses the penalty algorithm. General contact uses sliding mode which translates the tangential behavior. We have also defined the coefficient of friction, μ , which we will change to study its effect on the mechanical and electrical behavior of the phase. The hard contact has been defined so that the slave surface (slave node) cannot penetrate the "master" surface (master node) in the normal direction, but the reverse is possible (Figure 9).

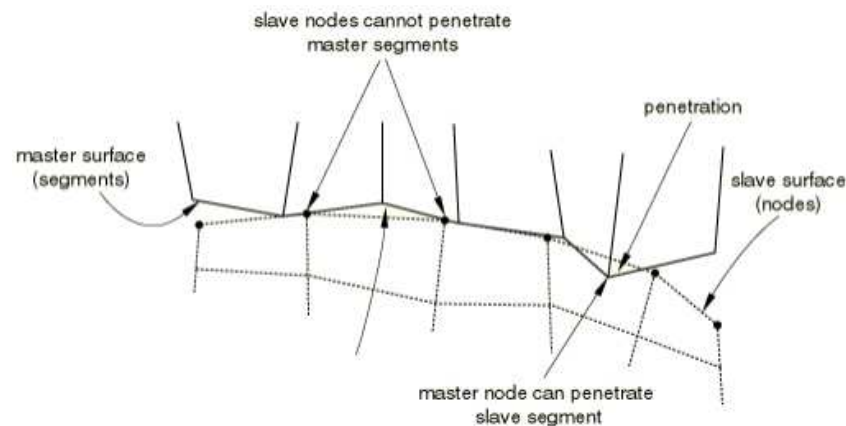


Figure 9. Rules of penetration of slave/master nodes [12].

2.5. Partial Conclusions and Assessment

The model created is a substantial model and allows us to model the mechanical behavior of the phase with different lengths and to numerically simulate its various damage mechanisms. Thanks to this FE model, non-linear effects such as contact, friction and plasticity, which are not integrated into the initial FE models of cables and which are very difficult to integrate into an analytical model, have been studied and this a significant innovation of this study. In addition, this model allows us to easily change the type of cable 1 + 6 to cable 1 + 6 + 12.

3. Results and Discussion

This part will start with the analysis of the mechanical behavior of the conductor under tensile and tensile-torsion loadings. Then, the effects of varying the coefficient of friction, the pitch, the work of hardening, the local plasticity and the breakage of a wire or several wires on the mechanical behavior of the conductor will be assessed.

3.1. Effect of Coefficient of Friction

The main objectives of this part are to understand the mechanical response of a phase to a combined loading under tension and under torsion by varying the coefficient of friction, and to assess the effect of friction between the wires in the case of a sound and damaged conductor with one or more broken wires. The coefficient of friction was varied, so the values considered are 0 for the ideal case (without friction), 0.05, 0.08, 0.1, 0.2 and 0.3. The pitch was fixed at 115 mm. An axial displacement, u_z of 3.5 mm, and a rotation θ_z of 0.35 radians on the end $Z = L$ were fixed. These conditions are applied with a smooth amplitude to remain within the quasi-static domain. In general, a lubricant is used to reduce the effects of friction in metallic structures. This is the case for HV submarine cables; the coefficient of friction between copper wires is between 0.1 and 0.2, but when a lubricant is used this coefficient drops to 0.05 and 0.08.

The mechanical behavior of a phase is a function of the coefficient of friction.

Figure 10 represents the curve of variation of axial force as a function of the deformation of the phase for the various values of the coefficient of friction. The numerical results are compared with the analytical results of the Costello and Labrosse model [13,14]. It is noted that the analytical results resulting from the solution of Costello and Labrosse [13–16] agree with our numerical results in the part of elasticity (linear part) and that the effect of the coefficient of friction is negligible on the behavior under tensile loading.

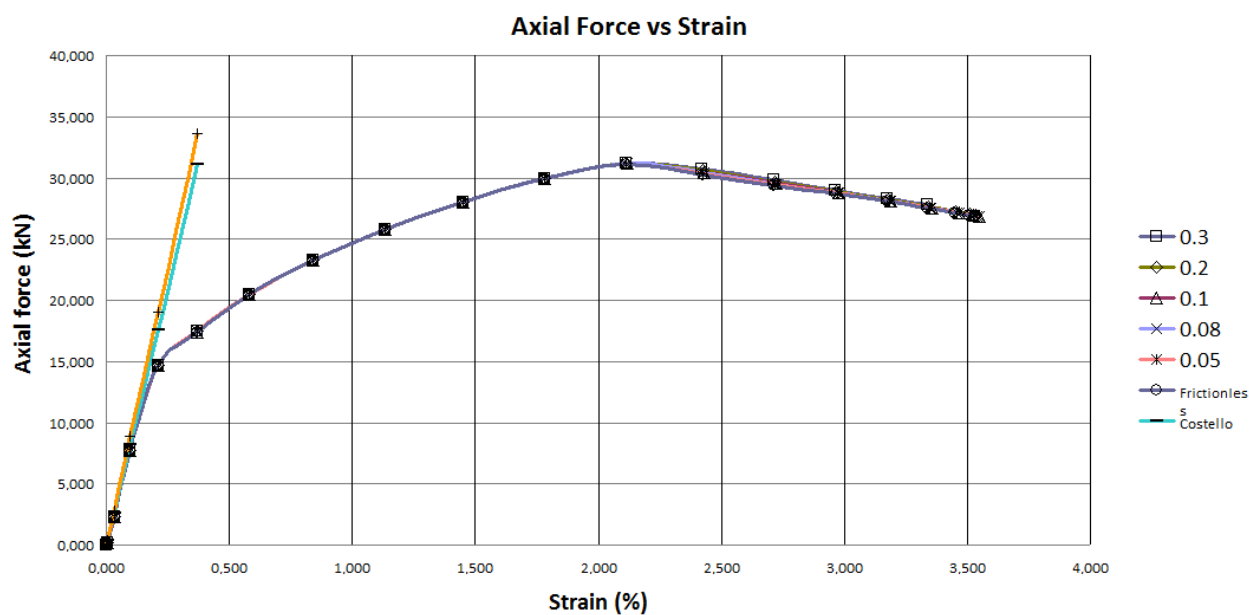


Figure 10. Axial force vs. strain.

The stress as a function of the deformation of the conductor is shown in Figure 11. The frictionless curve and the curves with different values of friction coefficients are identical for strains less than 2.1%. After this deformation, a small variation is seen. Although the variation is too small to be significant, it should be remembered that all these simulations are made under quasi-static conditions. Once fatigue kicks in, these small variations could lead to a huge impact on the conductor. Thus, in order to have a minimum influence of friction on the fatigue life of the conductor, they are manufactured with great care and refinement, so as to obtain a controlled inter-wire friction coefficient. It cannot be overlooked that during installation and operation the conductors experience maximum external forces, and during this period manufacturing defects can lead to excess roughness of the contact surfaces between the wires, which can result in high inter-wire friction forces.

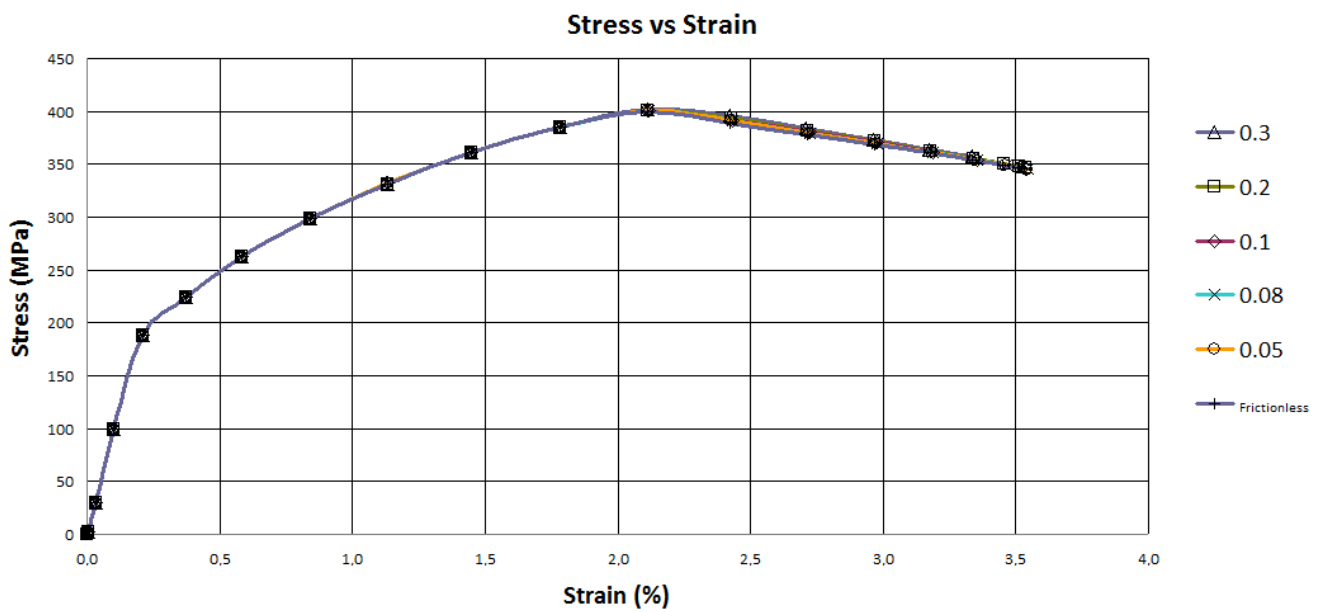


Figure 11. Stress-strain for various friction coefficients.

Figure 12 shows the variation of moment as a function of rotation. The numerical results are compared with the analytical results of the Costello and Labrosse model [13–15]. It is noted that the analytical results resulting from the solution of Costello agree with our numerical results in the linear part and that the effect of the coefficient of friction is negligible on the behavior of the phase in torsion. The core lines of contact and on the six helical wires are shown in Figure 13. As shown, the core experiences maximum line contact and therefore there is maximum risk of surface degradation along this line of contact.

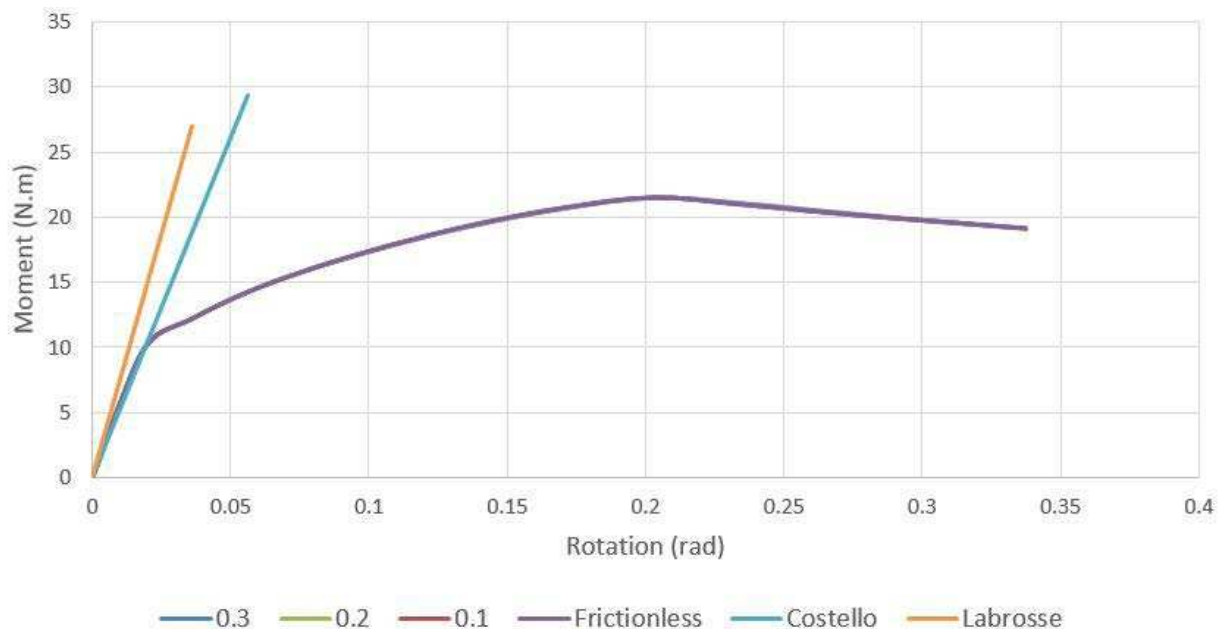


Figure 12. Torsion moment as a function of the rotation angle.

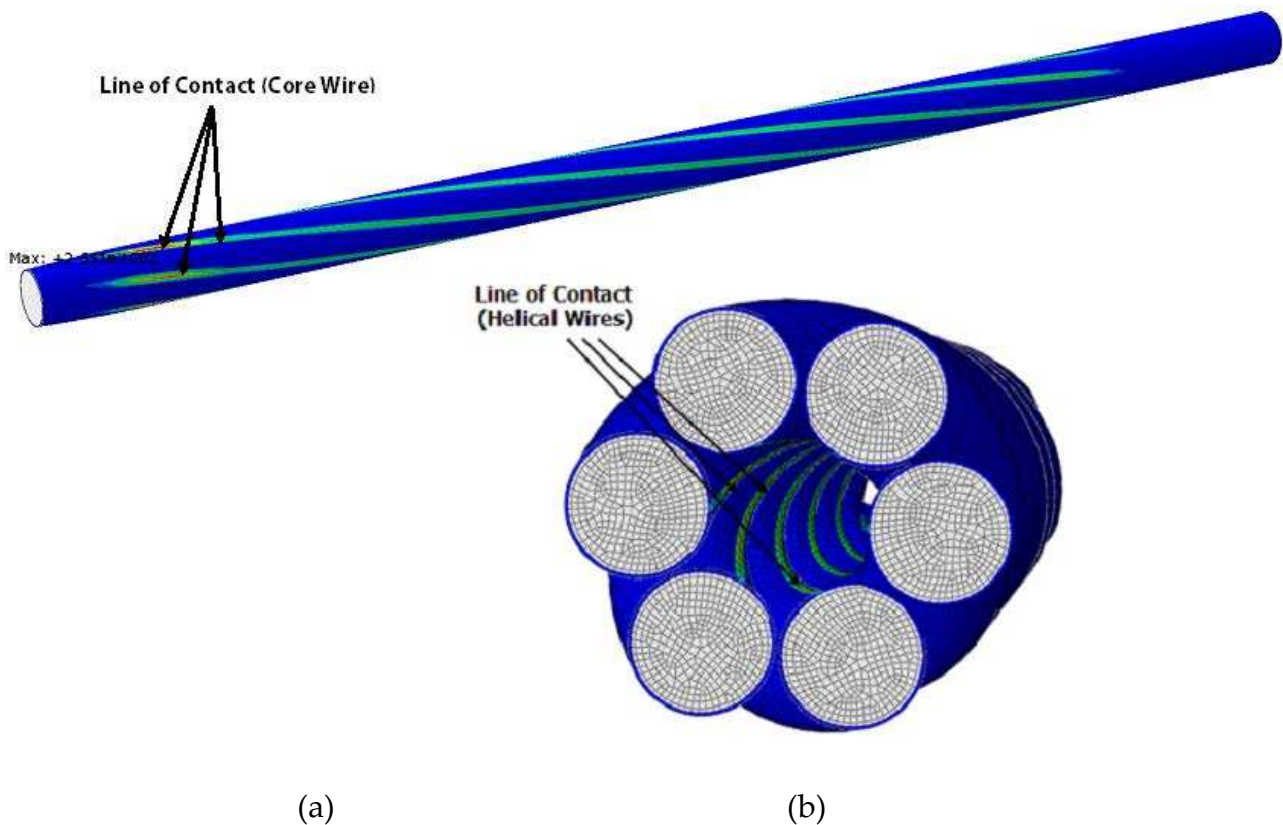
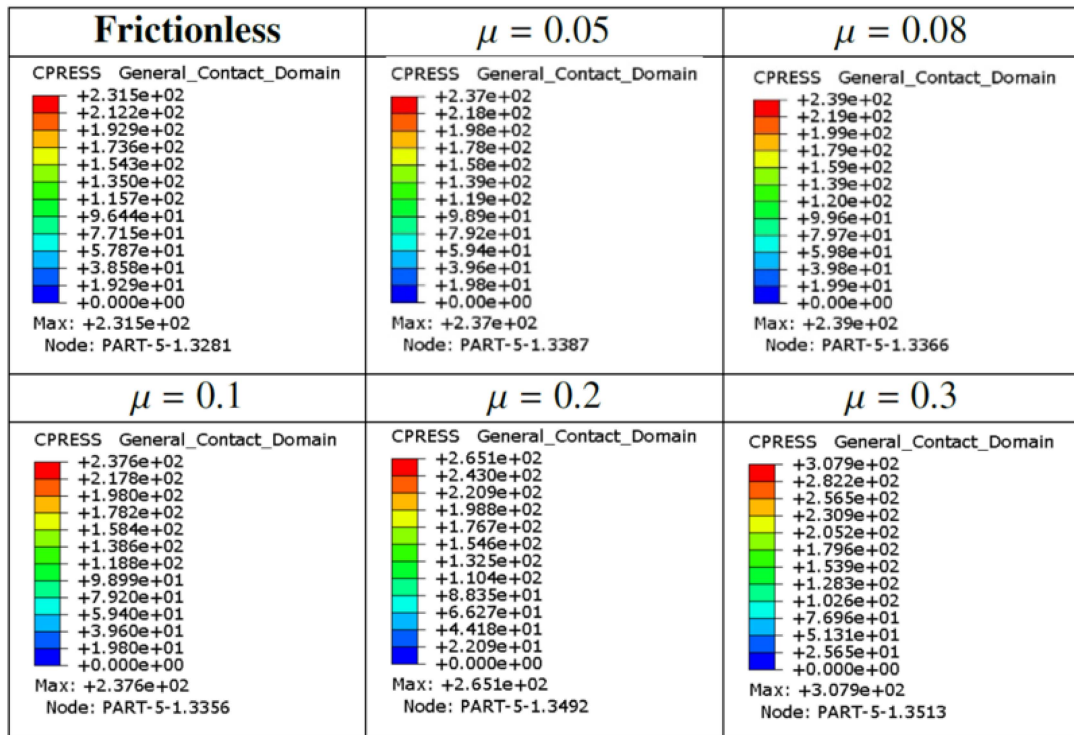


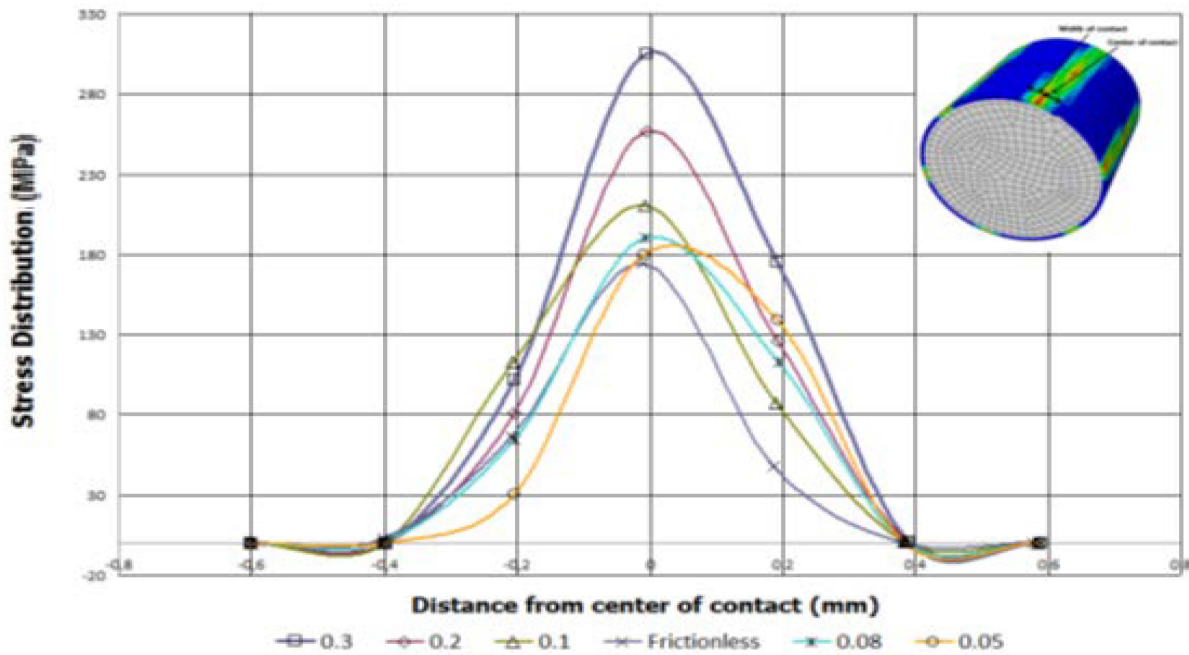
Figure 13. Contact line at the core-wire (a) and at the helical wire (b).

Figure 14a shows the contact pressure of the core in the cases where there is no friction and with friction. The maximum contact pressure without friction on the core is 231 MPa. It increases when the coefficient of friction increases. This is justified by the additional tangential pressure P_T in the case where there is friction. In a single 1 + 6 strand, the line of contact between the core and the helical wires is a helix, but locally it can be thought of as a contact between two parallel wires. Based on this assumption, Figure 14b shows the distribution of contact pressure over the contact width. The maximum pressure at the center of contact is 310 MPa for a coefficient of friction $\mu = 0.3$ and 190 MPa for $\mu = 0.05$. This seems an important result knowing that the core has a similar effect on its five other regions of the same contact width. This is why cable manufacturers apply lubricant between the wires to reduce friction effects.

Figure 15 shows the energy dissipated by friction which increases with increasing coefficient of friction. However, the energy dissipated by friction is in millijoules (mJ) for a quasi-static load, but under fatigue it will probably reach a value that will affect the material properties of the conductor and ultimately affect its conductivity, which would be detrimental technologically, economically and ecologically.



(a)



(b)

Figure 14. (a) Contact pressure for various friction coefficient; (b) Stress variation over the contact area.

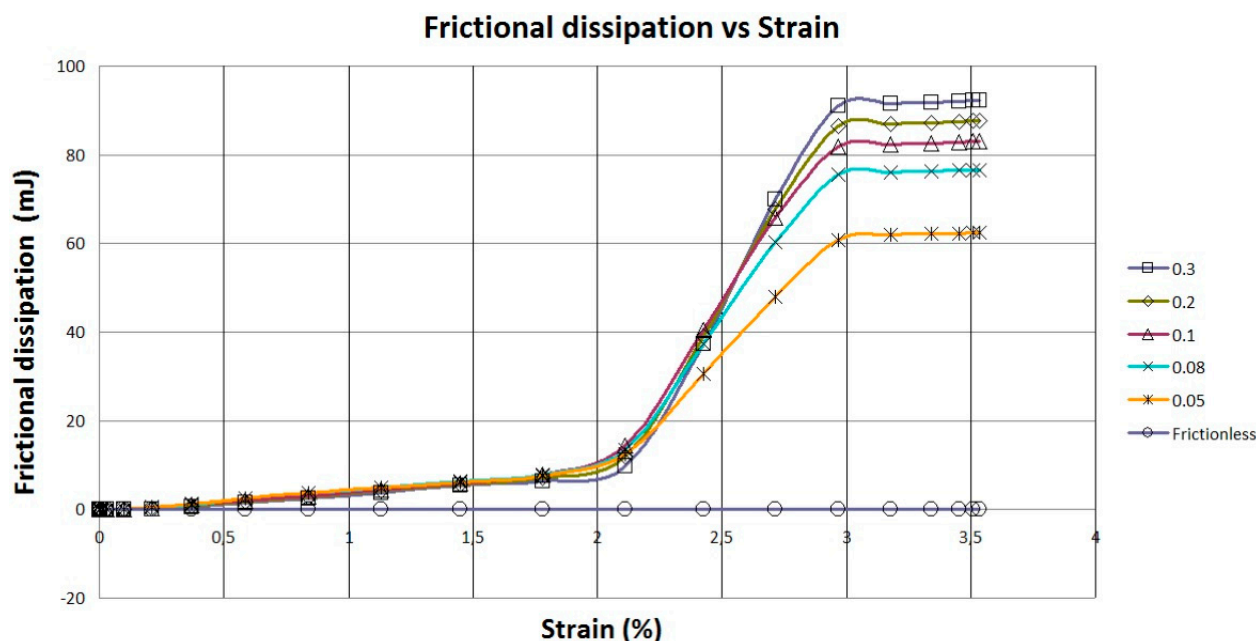


Figure 15. Dissipated friction energy as a function of strain for various friction coefficients.

3.2. The Effect of Friction in the Case of a Healthy or Damaged Conductor

We have seen the effect of the coefficient of friction in a healthy conductor. In this part, this effect is studied in the case of a damaged one, i.e., when a wire and/or several wires are broken. Although the situation of a broken wire is very rare and manufacturing companies take every precaution to avoid reaching this condition in an operating cable, a cable can nevertheless reach this damage scenario during its operation due to an external attack, or in the event of occasional damage. Keep in mind that the seabed has a steep surface, and that severe bending can occur with adverse consequences that can either plastically deform the conductor (one or more wires) or break it.

Figure 16 illustrates the variation of the energy dissipated by friction in the case of a healthy conductor, when one wire is broke, and a central wire is broken. The energy dissipated by friction in the case of the broken core is four times higher than that of the healthy conductor. The broken core creates a significant inter-wire differential sliding distance which generates this intense friction.

Figure 17 shows the variation of the energy dissipated by friction, of a conductor with a broken core with a variable coefficient of friction. The result is quite contradictory for the last part of the deformation where the energy dissipated for a coefficient of friction $\mu = 0.05$ is greater than the energy dissipated for $\mu = 0.3$. This result can be explained when considering that at large strain values, a phase where the core is broken, the energy dissipated by friction depends a little less on the coefficient of friction.

In the conductor, the sliding between the wires is of the elastic type. Therefore, the friction has almost zero amplitude and has little effect on the mechanical response of the axially loaded conductor. Once a wire is broken, undamaged threads begin to operate differential slip relative to the broken wire with significant friction (Figure 18). When both the core wire and a helical wire are broken, the differential slip distance is greater and therefore this intensifies the magnitude of friction. Thanks to the results of this model, one can imagine what would happen in a phase in which the breakage of one or more wires occur. The continuous or cyclic loadings (fatigue, creep) carried by the currents on the seabed will generate significant friction that can lead to the breakage of other wires, which could lead to a malfunction of the submarine cable.

To conclude, the results presented in this part show that the coefficient of friction has very little influence on the mechanical behavior under quasi-static loading. This effect is only interesting to evaluate in the case of cyclic loading. Moreover, results of the energy

dissipated by friction as a function of the deformation show that the coefficients of friction plays a role in the mechanical behavior of the damaged conductor.

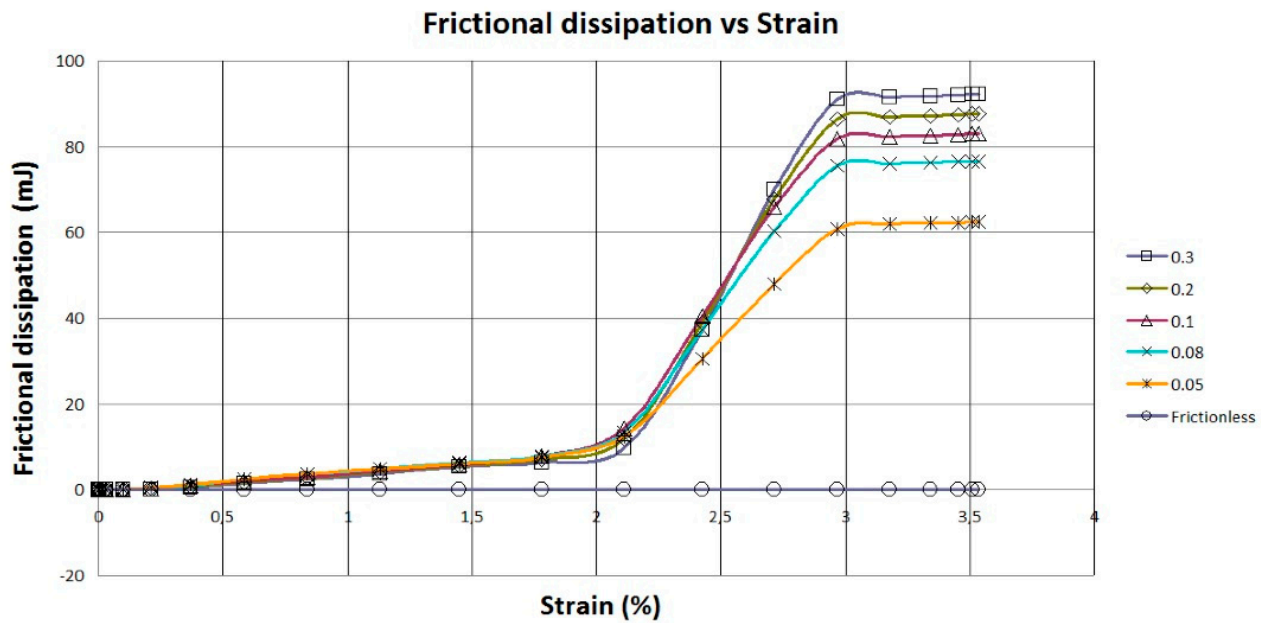


Figure 16. Comparison of dissipated friction energy of a healthy conductor with the case of one broken wire and the one where the core wire is broken.

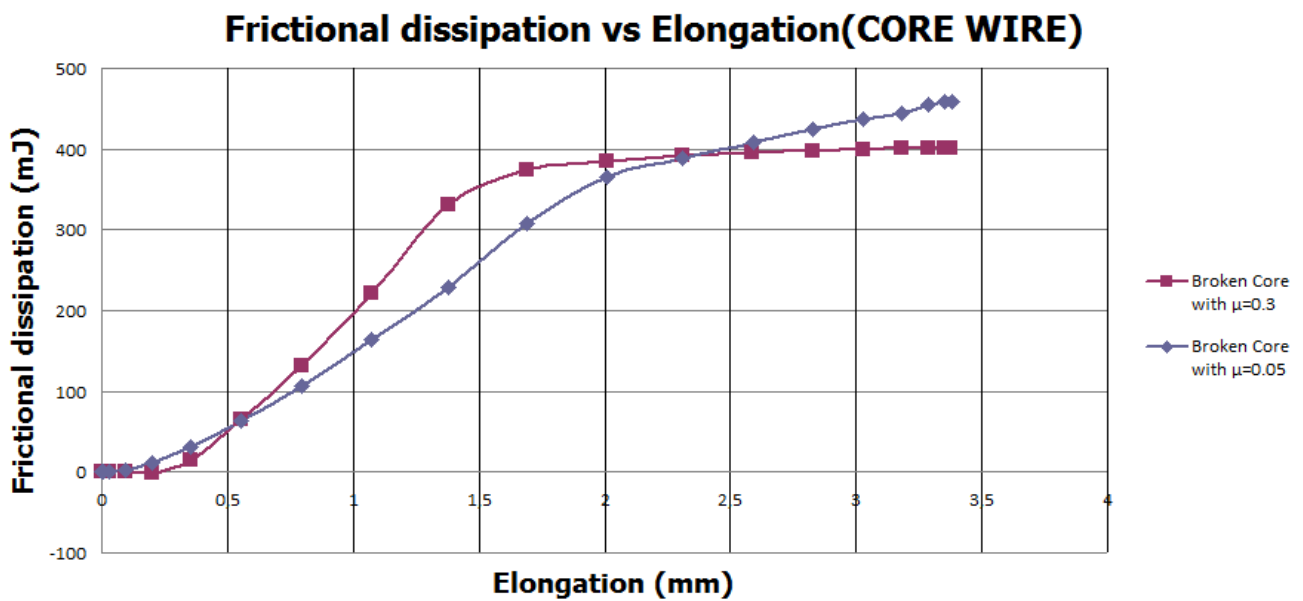


Figure 17. Dissipated friction energy for two different values of friction coefficient, for the case where the core wire is broken.

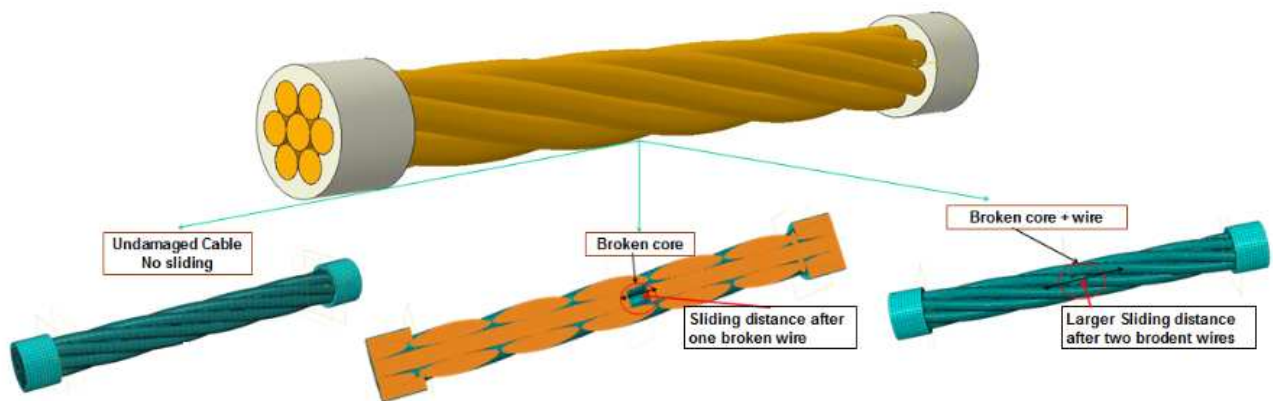


Figure 18. Various cases studied (healthy conductor), core-wire broken, one helical wire broken).

3.3. Pitch Effect

In this part, the effect of pitch on the mechanical behavior of the phase is studied. This parameter is among the parameters that determine the operation of the cable. It plays a very important role in mechanical, electrical and thermal behavior. We fixed all the parameters of our model except the pitch which is variable (Figure 19). The geometric parameters used in the model are conductor diameter (11.4 mm), diameter of core-wire (3.94 mm), diameter of helical wire (3.73 mm), conductor's length (115 mm) and pitch length (42 mm). The material parameters used in this study are the same as previously.

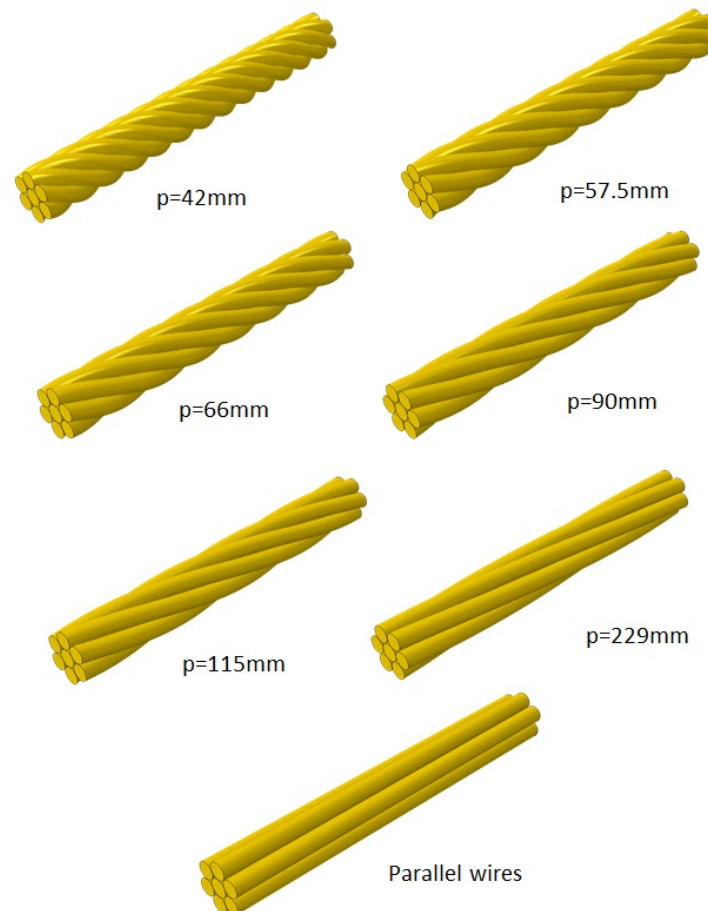


Figure 19. Conductor types with various pitch.

The contact part is defined by the coefficient of friction, which is 0.2 for the first study where we are only interested in the effect of the pitch. The second study of this part will compare the effect of pitch as a function of the coefficient of friction. So, for the second study, simulations with two quite distant friction coefficients (0.2 and 0.05) are made. The boundary conditions for all the simulations are one end fixed in all directions and an axial displacement of 40 mm on the other end. Figure 20 shows the mechanical response of the conductor for various pitch values. The results for the 229 mm pitch and the parallel wires are very close. The breaking stress of the conductor for small pitches is lower than the breaking stress for large pitches. These two observations can be explained by the fact that the resistance of conductors with large pitches is greater than the resistance in the conductors with small pitch values and that the inter-wire frictions are less in the conductors with large pitch. Low-pitch conductors are twisted. This is why when a conductor with a small pitch is subjected to an axial load, less force is required to cause it to break, as shown in Figure 20.

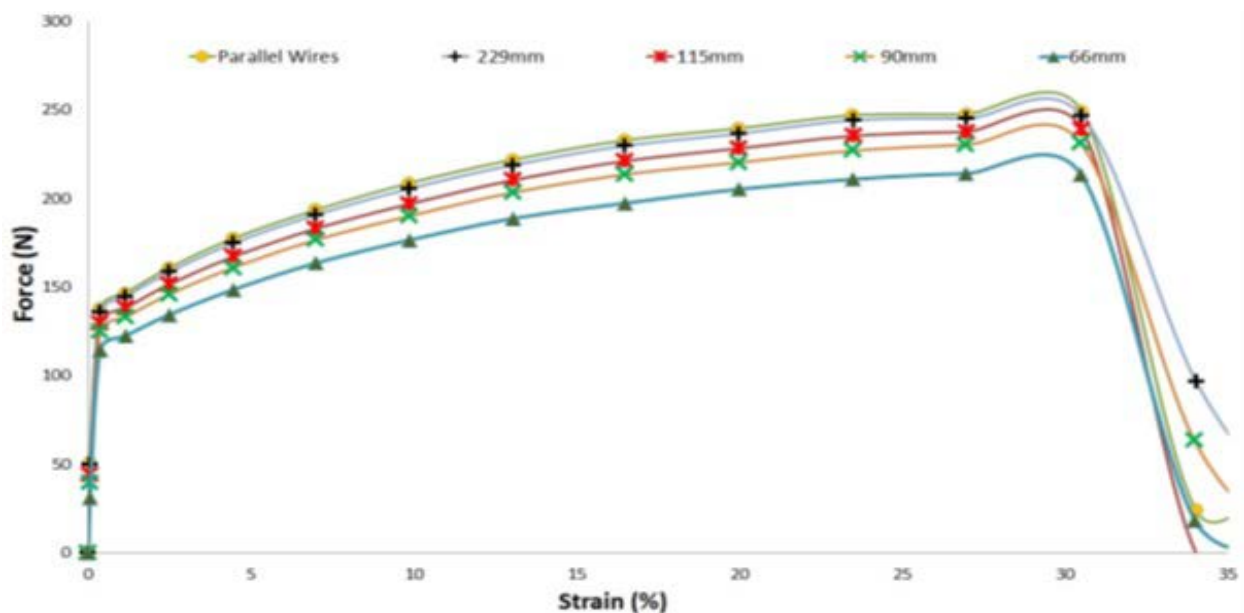


Figure 20. Simulated mechanical behavior of copper for various pitch values.

Figure 21 shows that the axial stiffness of the conductor, $k_{\epsilon\epsilon}$, increases when the pitch increases. Conductors with parallel wires have maximum axial tension compared to conductors with helical wires. Generally, conductors with parallel wires are not used as conductors due to their poor tensile stability, low torsion and low bending strength compared to stranded conductors. Therefore, most conductors are manufactured with a pitch of the order of 220 mm [17].

The numerical results (Figure 21) were compared with those derived from the analytical model of Labrosse. The results of the analytical model with boundary conditions similar to the numerical simulations are shown in Figure 22. These results are based on solutions of previous equations for various winding angles (or different pitches). By comparing Figures 21 and 22, the results of the numerical and analytical model are in good agreement for large pitches ($p \geq 115$ mm). With small pitches or large wrap angles, the difference between the results of the two models increases. Table 2 shows the difference in results between the numerical model and the analytical one. Indeed, in the analytical model of Labrosse, the effect of friction is not considered, but in the numerical model it is. Therefore, conductors with small pitches and a large contact region show a dispersion percentage greater than 34%.

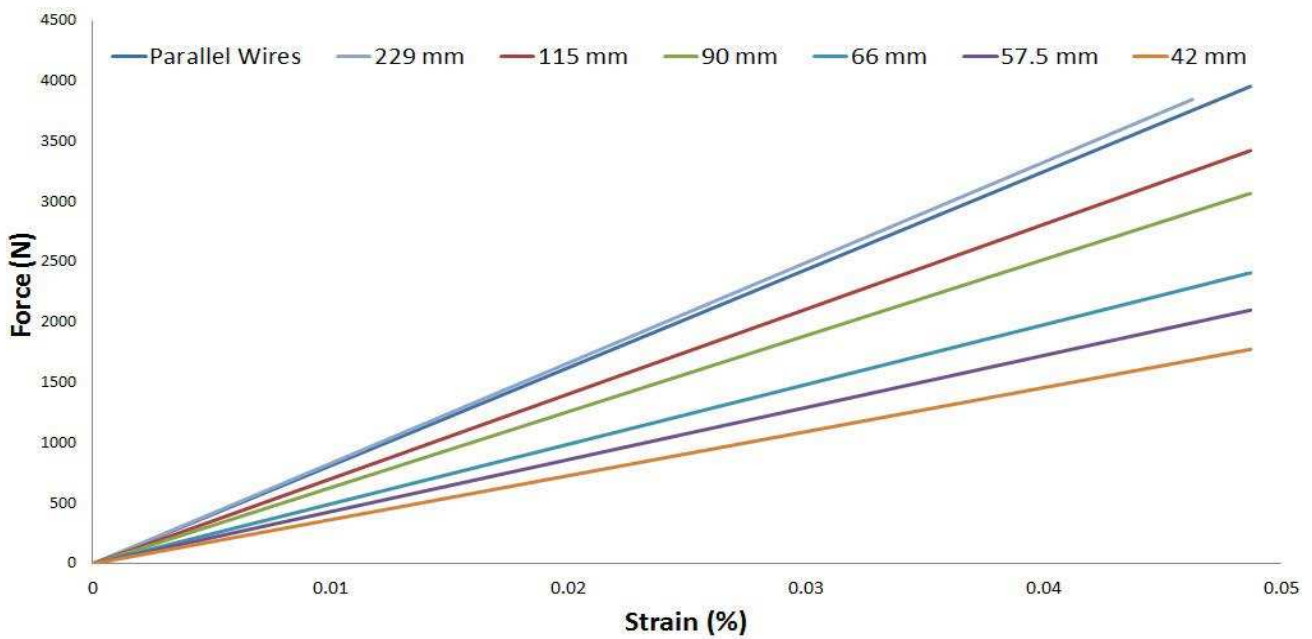


Figure 21. Variation of the elastic part of copper versus the pitch length (numerical results).

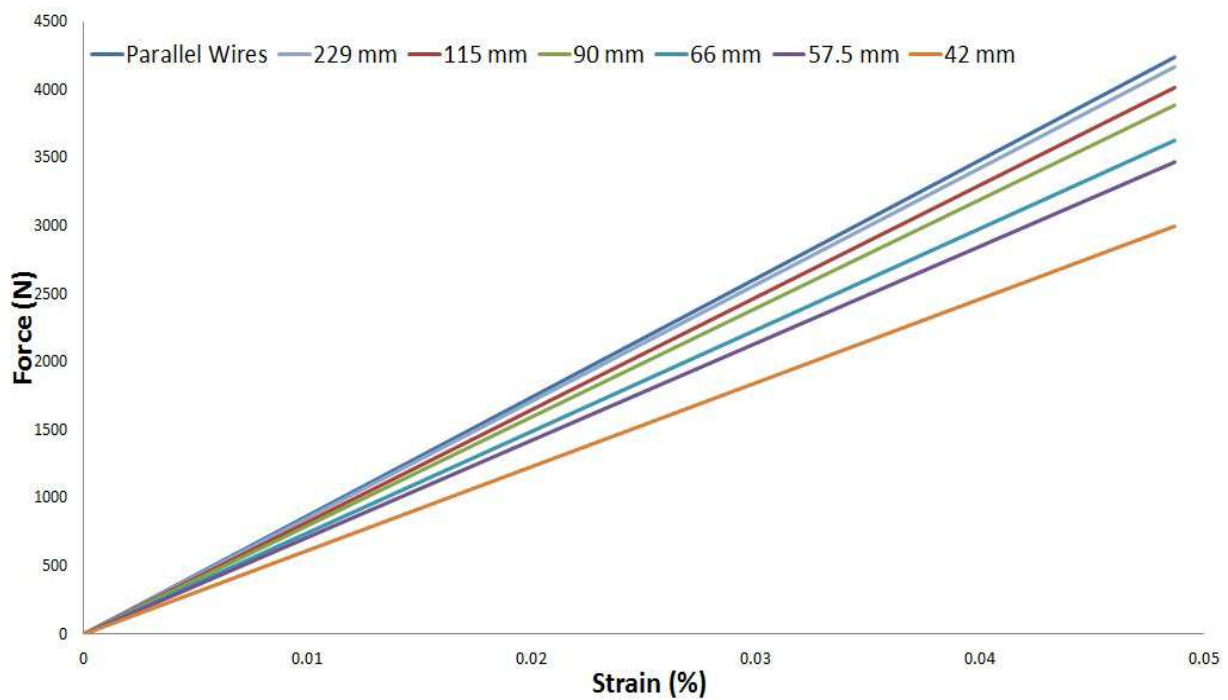


Figure 22. Conductor elastic area versus pitch length (analytical results).

Table 2. Conductor axial stiffness versus the pitch length (numerical and analytical).

Pitch (mm)	$k_{\epsilon\epsilon}$ Numerical (N)	$k_{\epsilon\epsilon}$ Analytic (N)	Scatter (%)
42	36,476	61,574	41
57.5	43,143	71,263	39
66	49,496	74,520	34
90	63,018	79,843	21
115	70,297	82,503	15
229	81,224	85,622	5
Very long	83,179	87,086	4

Underwater HV cables are manufactured with the aim of having minimum friction between the conductor wires to avoid any kind of unwanted heat dissipation, which can influence the operating conditions of the HV cable. When laying HV cables or during operation, the cables support different loads which can lead to inter-wire wear. With the onset of frictional forces, the energy dissipated by friction begins to be large enough to affect the resistivity of conductors. Figure 23 shows the frictional dissipated energy variation versus the pitch length, which allows us to study the dependence of the energy dissipated by friction on the pitch. The difference in the energy dissipated by friction of the cables with a pitch ≥ 115 mm is very small and it is only visible for large deformations. Cables with a pitch ≤ 57 mm begin to dissipate friction energy for small deformations. This behavior can be explained by the fact that the lines of contact between the core and the helical wires are much more numerous in the conductors with small pitches in comparison with conductors with larger pitches.

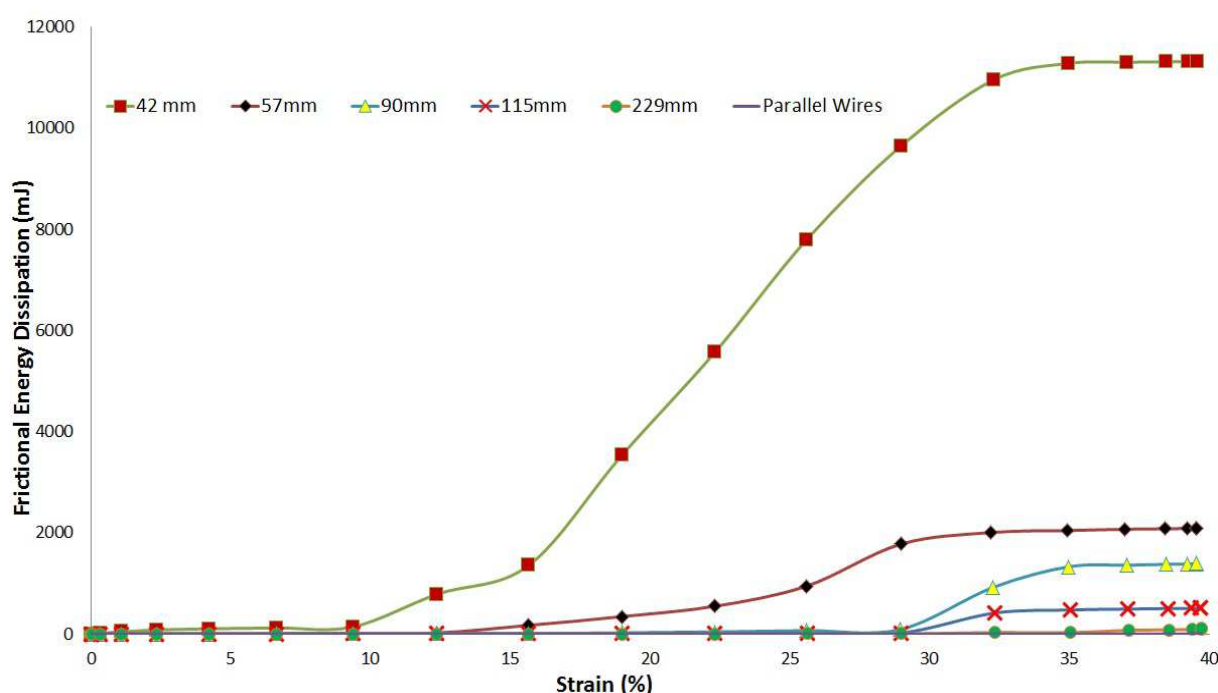


Figure 23. Frictional dissipated energy variation versus pitch length.

Figure 24, which displays frictional dissipated energy versus the pitch length and friction coefficient, illustrates the fact that cables with rougher surfaces lose higher energy dissipated by friction. The axial rigidity of the conductors is highest for the conductors of parallel wires and followed by the conductors of pitch equal to 229 mm. Similarly, the energy dissipated by friction as a function of the deformation shows that the pitch of the conductor and the coefficient of friction affect the mechanical behavior of the conductors. The energy dissipated by friction is minimal for conductors with parallel wires and conductors with pitch equal to 229 mm.

From the numerical results, it is clear that low-pitch conductors are strongly discouraged because of many disadvantages. Conductors with pitch equal to 229 mm or with parallel wires show almost similar numerical results, but due to their low tensile stability, torsional stiffness and bending strength, conductors with lower pitch are disadvantageous with regards to all aspects.

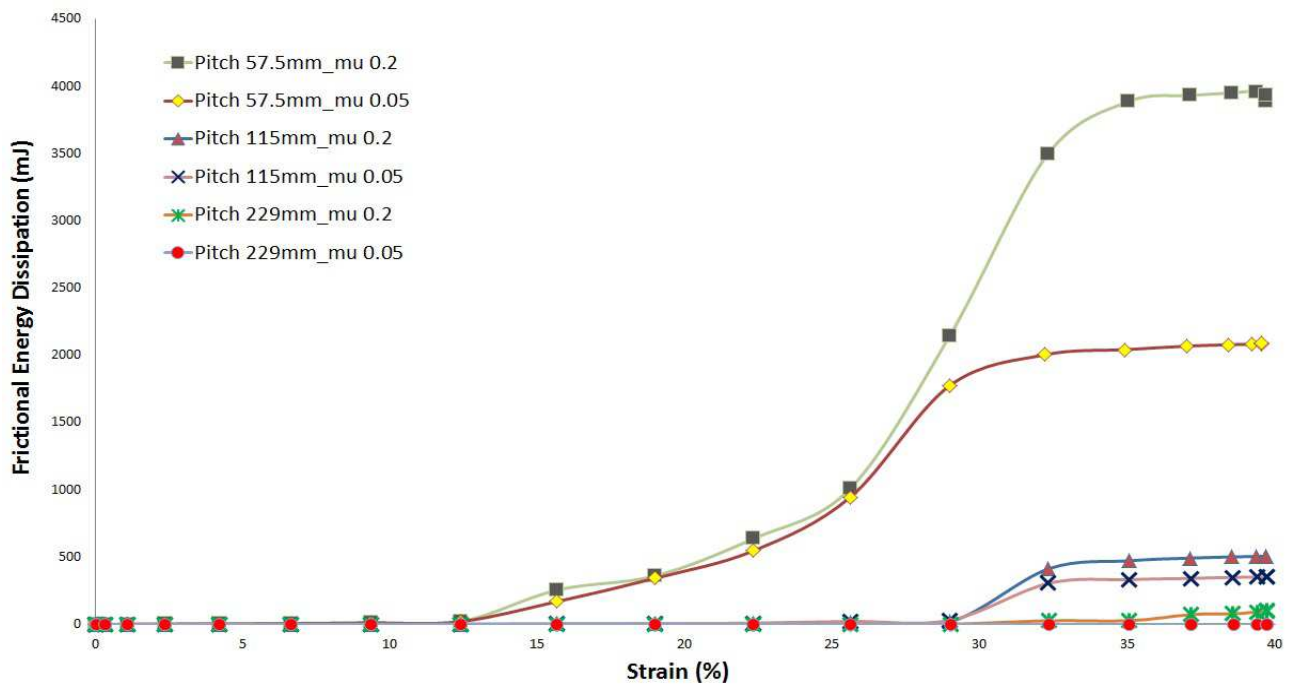


Figure 24. Frictional dissipated energy versus pitch length and friction coefficient.

3.4. Effect of Work-Hardening and Local Plasticity

During transport, installation and repair, HV submarine cables are subject to external forces which can be point-like. These forces can lead to local plastic deformation. In this part we studied the effect of this local deformation on the global behavior of the cable. We use the same model presented in the previous paragraphs and we will create a prestressed region in the core of the conductor. This prestressed region is created by applying pressure to a region of the core. Figure 25 shows how plasticity develops. The length of the region and the value of pressure applied determine the percentage of the defect with respect to the length of the conductor and the percentage of the local work-hardening, respectively.

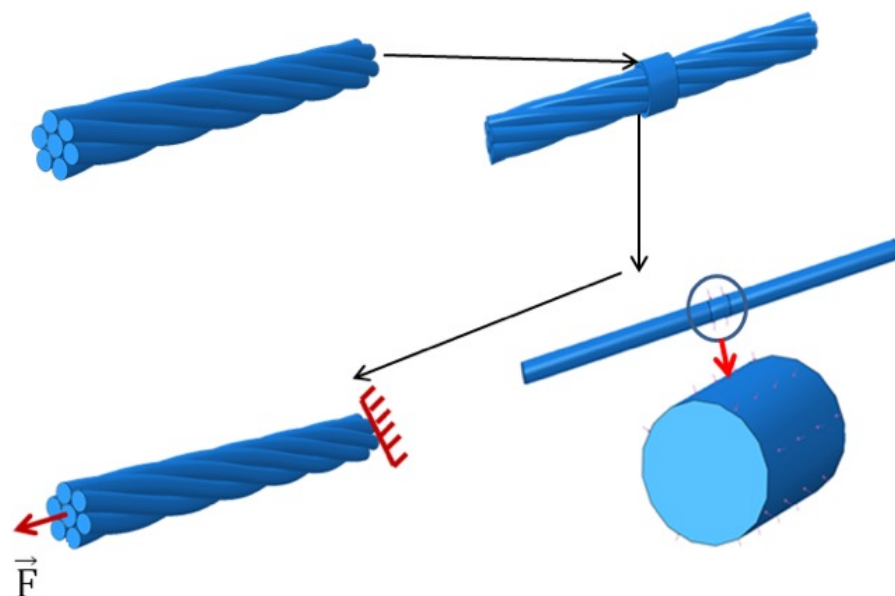


Figure 25. Illustration of local plasticity development.

The axial force-displacement curves obtained are a function of the percentage of work-hardening and the length of the prestressed region are depicted in Figure 26. It is noted that the percentage of local defect has no influence on the elastic stiffness. The nonlinear response of the conductor is influenced by the strain hardening percentage (Figures 26 and 27). Moreover, the slopes on the curves of Figure 27 show that there are successive wire breaks in the conductor with a local fault of 10% on the core wire.

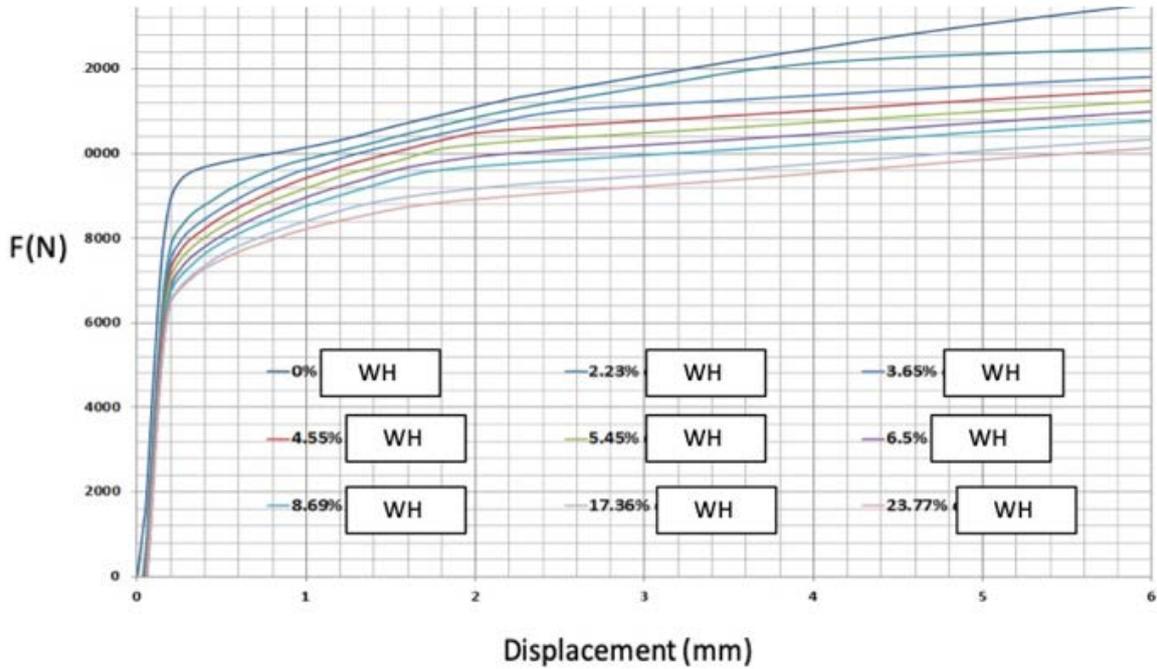


Figure 26. Work-hardening effect on the conductor with a 5% defect on the core wire (WH refers to Work-Hardening).

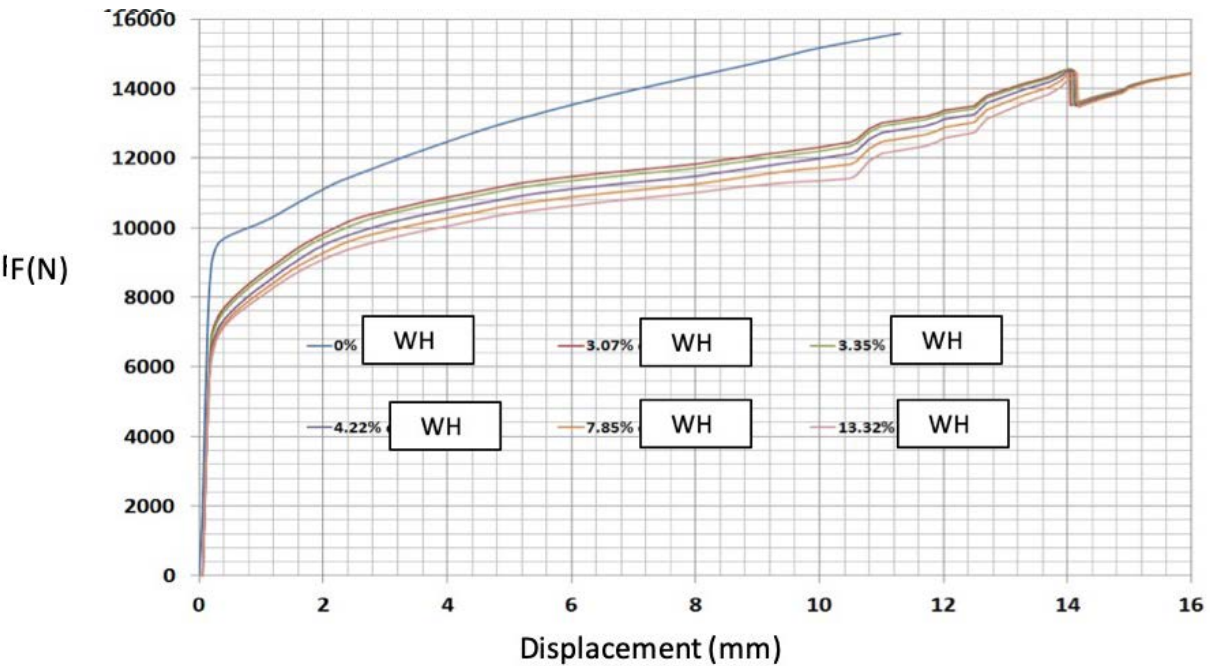


Figure 27. Work-hardening vs. the behavior of the phase with 10% local defect at the core wire (WH refers to Work-Hardening).

This work, which was carried out numerically from start to finish [18] will serve as an introductory study to a phase system composed of a very soft metal which is very difficult to study, given its deformability and the fine size of the wires. On the basis of the results obtained, new research is planned and will relate to the micro-mechanical analysis of the behavior of the wires of the phase, highlighting two aspects. The first is dedicated to the behavior of inter-wire friction, while the second will focus on the progressive plasticity of the yarns on their mechanical behavior. These two aspects will be studied by instrumented micro-indentation (see for example [19,20]). Note that valuable work devoted to light-weight metals can be a good source of additional information [21].

4. Conclusions

The work carried out in this article is part of the National Project EMODI as well as the European Project FLOW-CAM. A model has been proposed to evaluate the effects of damage mechanisms on the mechanical behavior of the high-voltage phase for offshore. This model started from scratch as no literature exists so far and most of the existing studies are dedicated to steel wires, which are very different from copper wires. This model has the advantage of taking into consideration the effects of inducing a non-linear mechanical behavior (work-hardening, sliding/friction or wire breakage) [19]. The proposed model, which uses for many aspects the modules of Abaqus, constitutes for us only an introduction to further studies of the very fine aspects relating to the damage micro-mechanisms operating within the wires in high-voltage phases. In this respect, this research only claims to have made very modest advances. The objectives were to identify the mechanisms of damage and to estimate their preliminary effects on the behavior of the phase. In a future study, our research will aim to go more in-depth on each of the micro-mechanisms and to evaluate more precisely their effects on the overall mechanical behavior of the whole, while being aware that this model, although taking into consideration the aforementioned mechanisms, is nonetheless incomplete because it does not describe the behavior under cyclic fatigue. It should be kept in mind that the computation times are too long to be considered within current research parameters and that, as is well-known, many efforts are underway to provide alternative options that may reduce calculation times. Techniques for circumventing the difficulties are showing up; however, we do not currently have the means to segregate one that is physically relevant. Another point should be made relating to experimental validation. This has not yet been performed, since the goal of the study was nothing but introductory.

Author Contributions: F.E.-C. contributed to analysis, investigation and calculation. M.D.-H. is responsible for methodology, supervision, project administration and funding acquisition. The authors have read and agreed to the published version of the manuscript. All authors have read and agreed to the published version of the manuscript.

Funding: This research received funding from FLOW-CAM (Floating Offshore Wind turbine Cable Monitoring) EraNet MarTERA Project.

Institutional Review Board Statement: Not applicable.

Informed Consent Statement: Not applicable.

Data Availability Statement: Data is available.

Acknowledgments: M.D.-H. acknowledges the funding of F.E.-C. by the Local Government of Pays de La Loire, as well as by the FLOW-CAM Project (ERA-NET).

Conflicts of Interest: The authors declare no conflict of interest.

References

1. Drissi-Habti, M.; Neginhal, A.; Manepalli, S.; Carvelli, V.; Bonamy, P.-J. Concept of Placement of Fiber-Optic Sensor in Smart Energy Transport Cable under Tensile Loading. *Sensors* **2022**, *22*, 2444. [CrossRef] [PubMed]
2. Drissi-Habti, M.; Neginhal, A.; Manepalli, S.; Carvelli, V. Fiber-Optic Sensors (FOS) for Smart High Voltage Composite Cables—Numerical Simulation of Multi-Parameter Bending Effects Generated by Irregular Seabed Topography. *Sensors* **2022**, *22*, 7899. [CrossRef] [PubMed]
3. Drissi-Habti, M.; Raman, V.; Khadour, A.; Timorian, S. Fiber Optic Sensor Embedment Study for Multi-Parameter Strain Sensing. *Sensors* **2017**, *17*, 667. [CrossRef] [PubMed]
4. Raman, V.; Drissi-Habti, M. Numerical simulation of a resistant structural bonding in wind-turbine blade through the use of composite cord stitching. *Compos. Part B Eng.* **2019**, *176*, 107094. [CrossRef]
5. Raman, V.; Drissi-Habti, M.; Limje, P.; Khadour, A. Finer SHM-Coverage of Inter-Plies and Bondings in Smart Composite by Dual Sinusoidal Placed Distributed Optical Fiber Sensors. *Sensors* **2019**, *19*, 742. [CrossRef]
6. Gulski, E.; Anders, G.J.; Jongen, R.A.; Parciak, J.; Siemiński, J.; Piesowicz, E.; Paszkiewicz, S.; Irska, I. Discussion of electrical and thermal aspects of offshore wind farms' power cables reliability. *Renew. Sustain. Energy Rev.* **2021**, *151*, 111580. [CrossRef]
7. Nawrocki, A. In French Contribution à la Modélisation Des Câbles Monotorons par Eléments Finis. Ph.D. Thesis, Ecole Centrale de Nantes, Nantes, France, 1997.
8. Carlson, A.D.; Kasper, R.G. *A Structural Analysis of a Multiconductor Cable*; Rapport Technique AD-767 963; Naval Underwater System Center, New London Laboratory: London, UK, 1973.
9. Cutchins, M.A.; Cochran, J.E.; Guest, S.; Fitz-Coy, N.G.; Tinker, M.L. An investigation of the damping phenomena in wire rope isolator. The Role of Damping in Vibration and Noise Control. In Proceedings of the 1987 ASME Design Technology Conference, Boston, MA, USA, 27–30 September 1987; Volume 5, pp. 197–204.
10. Chiang, Y.J. Characterizing simple-stranded wire cables under axial loading. *Finite Elem. Anal. Des.* **1996**, *24*, 49–66. [CrossRef]
11. Jiang, W.G.; Yao, M.S.; Walton, J.M. A concise finite element model for simple straight wire rope strand. *Int. J. Mech. Sci.* **1999**, *41*, 143–161. [CrossRef]
12. *Abaqus/Explicit User's Manual, Section 13, Quasi-Static Analysis with Abaqus Explicit, Volume II*; Dassault Systems Simulia Corp: de la Madeleine, France, 2012.
13. Hertz, H. On the contact of elastic solids. *J. Reine Angew. Math.* **1882**, *92*, 156–171. [CrossRef]
14. Costello, G.A. *Theory of Wire Rope*, 2nd ed.; Springer: Berlin/Heidelberg, Germany, 1997.
15. Labrosse, M. Contribution à L'étude du Rôle du Frottement sur Le Comportement et la Durée de Vie des Câbles Monocouches. Ph.D. Thesis, Ecole Centrale de Nantes, Nantes, France, 1998.
16. Labrosse, M.; Nawrocki, A.; Conway, T. Influence of friction on the cyclic response of simple straight wire rope strands under axial loads. *Tire Sci. Technol.* **2000**, *28*, 233–247. [CrossRef]
17. Available online: https://www.cic-cables.com/wa_files/GENERAL_2022_web.pdf (accessed on 26 January 2022).
18. Ech-Cheikh, F. Numerical and analytical modeling of the mechanical and multiphysics behavior of a phase of Hi-Voltage electrical cable for offshore farms. Ph.D. Thesis, Ecole Centrale Nantes, Nantes, France, 26 January 2022.
19. Drissi-Habti, M.; Nakano, K. Microstructure and mechanical properties of Hi-Nicalon/BN/ α -silicon-nitride ceramic-matrix composites. *Composites Sci. Tech.* **1997**, *57*, 1483–1489. [CrossRef]
20. Drissi-Habti, M.; Nakano, K. Local mechanical characterisation and modelling of the interfacial behaviour in Hi-Nicalon/BN/ α -Si₃N₄ ceramic matrix composites by way of instrumented microindentation tests. *J. Eur. Ceram. Soc.* **1998**, *18*, 1845–1855. [CrossRef]
21. Deng, Y.; Liang, X.; Cao, Z.; Kong, L.; Wang, C.; Ruan, Y.; Zheng, X. The Analysis of Mechanical Properties and Lightweight Design of Nonmetallic Armored Umbilical Cable. *J. Press. Vessel. Technol.* **2022**, *144*, 51301. [CrossRef]

Disclaimer/Publisher's Note: The statements, opinions and data contained in all publications are solely those of the individual author(s) and contributor(s) and not of MDPI and/or the editor(s). MDPI and/or the editor(s) disclaim responsibility for any injury to people or property resulting from any ideas, methods, instructions or products referred to in the content.